The EMBO Journal Vol. 22 No. 1 pp. 70–77, 2003

Repeat motifs of tau bind to the insides of microtubules in the absence of taxol

Santwana Kar, Juan Fan, Michael J.Smith, Michel Goedert and Linda A.Amos[1]

MRC Laboratory of Molecular Biology, Hills Road, Cambridge CB2 2QH, UK

[1]Corresponding author
e-mail: laa@mrc-lmb.cam.ac.uk

The tau family of microtubule-asssociated proteins has a microtubule-binding domain which includes three or four conserved sequence repeats. Pelleting assays show that when tubulin and tau are co-assembled into microtubules, the presence of taxol reduces the amount of tau incorporated. In the absence of taxol, strong binding sites for tau are filled by one repeat motif per tubulin dimer; additional tau molecules bind more weakly. We have labelled a repeat motif with nanogold and used three-dimensional electron cryomicroscopy to compare images of microtubules assembled with labelled or unlabelled tau. With kinesin motor domains bound to the microtubule outer surface to distinguish between α- and β-tubulin, we show that the gold label lies on the inner surface close to the taxol binding site on β-tubulin. Loops within the repeat motifs of tau have sequence similarity to an extended loop which occupies a site in α-tubulin equivalent to the taxol-binding pocket in β-tubulin. We propose that loops in bound tau stabilize microtubules in a similar way to taxol, although with lower affinity so that assembly is reversible.

Keywords: kinesin/microtubule-associated proteins (MAPs)/taxol/three-dimensional image reconstruction/tubulin

Introduction

Microtubules assembled from αβ-tubulin heterodimers are labile polymers unless stabilized by other molecules. The anti-cancer drug taxol does this by binding to a specific site on β-tubulin, on the inside of a microtubule, where it is thought to influence interactions between adjacent subunits (Nogales *et al*., 1999). Structural microtubule-associated proteins (MAPs), such as tau, also maintain the stability of tubulin polymers. The repeat motifs found in the microtubule-binding domain of tau are conserved from nematodes and fruit flies to humans (Goedert *et al*., 1996; Heidary and Fortini, 2001) and have 60–70% sequence similarity to motifs in other MAPs such as the high molecular weight neuronal MAP2 and the more widespread MAP4. Tau is widely expressed in the nervous system, where it plays an essential role; although mice that are deficient in either tau alone or MAP1B alone appear normal, those lacking both MAPs show neuronal defects and die by 4 weeks of age (Takei *et al*., 2000). In humans, hyperphosphorylated tau can assemble into abnormal filaments characteristic of Alzheimer's and other neurodegenerative diseases (Lee *et al*., 2001). Mutations in or close to the repeat region cause inherited frontotemporal dementia and parkinsonism linked to chromosome 17 (FTDP-17) (Hutton *et al*., 1998; Poorkaj *et al*., 1998; Spillantini *et al*., 1998). Functionally, such mutations often reduce the ability of tau to promote microtubule assembly (Hasegawa *et al*., 1998). The six isoforms of human brain tau are alternatively spliced from a single gene and differ by having three or four conserved repeat motifs in the microtubule-binding domain and no, one or two insertions in the N-terminal projection domain (Figure 1A). The repeats (Figure 1B) have microtubule-binding and assembly-promoting activity, while the regions flanking them have binding affinity but do not promote assembly (Trinczek *et al*., 1995). 3R-tau and 4R-tau are developmentally regulated and imbalances in their ratios can lead to FTDP-17 (Hutton *et al*., 1998; Spillantini *et al*., 1998), indicating that each isoform has distinct roles.

Hitherto, studies of tau–tubulin interactions have involved peptides of tau or tubulin reacting under non-physiological conditions, or whole tau molecules or fragments binding to preformed taxol-stabilized microtubules (Littauer *et al*., 1986; Melki *et al*., 1991; Gustke *et al*., 1994; Chau *et al*., 1998; Al-Bassam *et al*., 2002). It has been reported that, when tau or other MAPs are added to microtubules which have already been assembled into closed tubes and stabilized, they bind to the outer surface in a specific manner (Chau *et al*., 1998; Ackmann *et al*., 2000; Al-Bassam *et al*., 2002). We have investigated the interaction of whole tau co-assembled with microtubules in the absence of taxol and have found that tau binds more tightly than when taxol is present. Taxol is known to bind to a site on β-tubulin on the inside of a microtubule where α-tubulin has a conserved extra loop (Nogales *et al*., 1999). We have labelled a repeat motif in the microtubule-binding domain of tau with nanogold and located the label on microtubules by three-dimensional electron cryomicroscopy. The results indicate that under our assembly conditions a repeat motif occupies a similar site to taxol. Since tubulin cannot have evolved to bind taxol, we believe that our work finally answers the question of what type of natural substrate binds to this pocket in β-tubulin.

Results

The possibility that a tau repeat might bind to a site on β-tubulin that overlaps the taxol site was initially suggested by sequence similarity between tau repeats and the extended loop in α-tubulin (Figure 1B) which fills a pocket similar to the taxol site (Nogales *et al*., 1999).

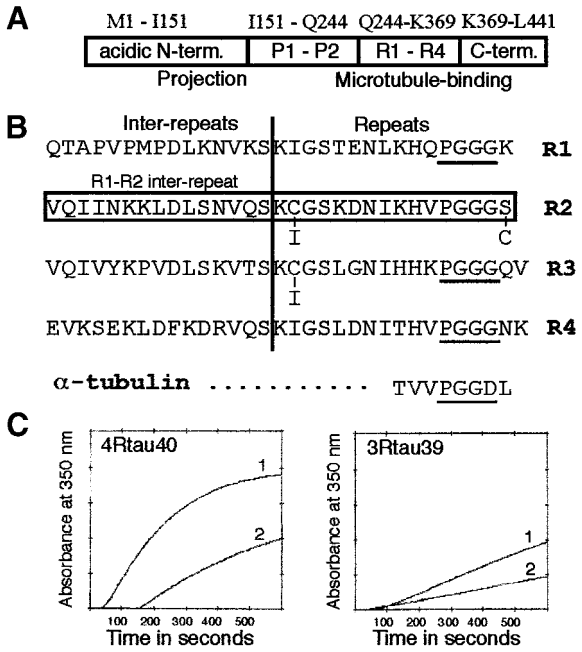

Fig. 1. Comparison of differences in tau proteins. (**A**) Diagram of four-repeat tau (4R-tau) molecule. The N-terminal segment forms a projection from a microtubule when the rest of the molecule is bound (Hirokawa *et al*., 1988). R1–R4 repeat motifs are flanked by proline-rich (P1–P2) and C-terminal segments. 3R-tau is similar apart from lacking one of the repeat motifs. (**B**) Amino acid sequence of the four repeats in one-letter code. Mutation sites C291I, C322I and S305C are indicated. Boxed sequence (V275–S305) is absent from three-repeat tau (3R-tau). The sequence from α-tubulin (T361–L368) is an extra loop filling the equivalent of the taxol site. (**C**) Spectroscopic assay of microtubule assembly with 4R-tau and 3R-tau, each purified by two methods (see text).

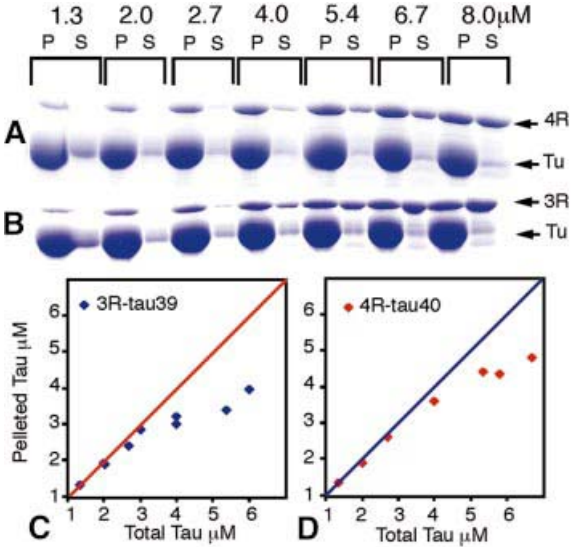

Fig. 2. Pelleting assays. (**A** and **B**) SDS–polyacrylamide gels showing proteins in pellets (P) and supernatants (S) when 10 μM tubulin dimer was incubated with increasing concentrations of either triple mutant 4R-tau (A) or wild-type 3R-tau (B). Tau runs anomalously above tubulin (Tu) on gels. Wild-type 4R-tau (see Figure 3) and the mutant (shown here and in Figure 5C) gave indistinguishable results. (**C** and **D**) Plots of pelleted tau measured by densitometry of gels such as those in (A) and (B). The points diverge first gradually, then much more rapidly, from the diagonal lines as increasing proportions of tau appear in the supernatant.

We purified recombinant proteins as described previously (Smith *et al*., 2000), choosing two tau isoforms: a 45.8 kDa molecule (4R-tau) with four repeats (Figure 1) and a 42.6 kDa molecule (3R-tau) with three repeats. Both were tested for activity in assembly assays (Figure 1C), since we found that tau purified by some methods can have low activity even if the protein is pure and binds well to microtubules in pelleting assays. We used only fully 'active' tau for most experiments and included trimethylamine-*N*-oxide (TMAO) in all our buffers, since this and other osmolytes enhance the effect of tau on tubulin assembly (Tseng and Graves, 1998; Smith *et al*., 2000). To stabilize microtubules further during the preparation of samples for electron microscopy, we added GMPCPP, an analogue of GTP that is only slowly hydrolysed (Hyman *et al*., 1992).

Pelleting assays were carried out with a constant amount of tubulin and varying amounts of 4R-tau or 3R-tau. Under the conditions used, very low tau concentrations failed to stimulate the assembly of a large fraction of the tubulin, which remained in the supernatant, whereas at tau concentrations >1 μM most of the tubulin appeared in the pellets (Figure 2A and B). Plots of the amounts of tau in the pellets (Figure 2C and D) show strong binding (estimated dissociation constant ~10^{-7} M) at low ratios of tau to tubulin. Tau started to appear in the supernatant sooner for 3R-tau than for 4R-tau. The strong binding range of 3R-tau to tubulin is up to one tau molecule per three tubulin dimers (~3.3 μM 3R-tau to 10 μM tubulin dimers) (Figure 2C). At higher ratios, the gradient of the curve is less steep, indicating weaker binding (~10^{-6} M). Strong binding of 4R-tau persisted as far as one tau molecule per two to three tubulin dimers (~4 μM 4R-tau to 10 μM tubulin dimers) (Figure 2D).

The acidic C-terminal residues of tubulin have been shown to interact with MAPs (Serrano *et al*., 1984; Chau *et al*., 1998), although binding is not abolished by loss of these residues. To investigate the importance of their role in binding tau of known activity, we repeated some experiments with tubulin whose C-termini had been removed by subtilisin digestion (S-tubulin). It was necessary to prepare S-tubulin in the presence of taxol to ensure its stability during complete modification of both α- and β-tubulin (Serrano *et al*., 1984) (Figure 3A), which meant that we could not test tau-induced assembly in the complete absence of taxol. The binding of 3 μM active 4R-tau and 3 μM active 3R-tau to S-tubulin microtubules is shown in Figure 3B. We estimate that, compared with normal tubulin and 20 μM taxol, binding of active 4R-tau was reduced by 15% and binding of active 3R-tau by 28%. The loss was greater, but still not complete, for less active 3R-tau (Figure 3C). Native MAP2 reacted in a similar way to active recombinant tau (Figure 3B).

Binding assays carried out with tau and normal tubulin in the presence of kinesin and AMP-PNP (Figure 3D) produced no significant difference in the amount of tau pelleted, showing that strongly bound kinesin does not compete with tightly bound tau. Furthermore, the amount of kinesin bound was the same whether it was added before or after microtubule assembly (not shown).

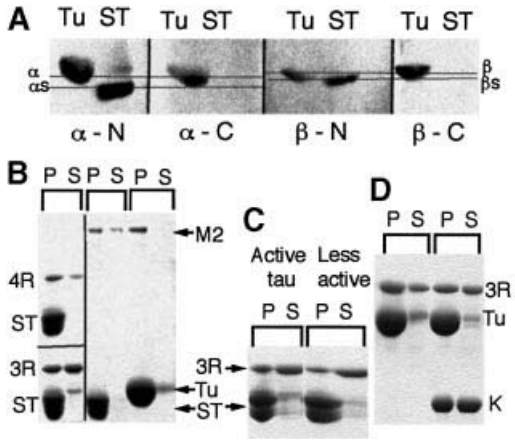

Fig. 3. (**A**) Western blots of SDS gels, with lanes containing undigested tubulin (Tu) and subtilisin-digested tubulin (ST), incubated with four different anti-tubulin monoclonal antibodies specific to either α- or β-tubulin; the epitopes lie either at the very C-termini or closer to the N-termini. (**B**) SDS gels showing 3.0 μM wild-type 3R- and 4R-tau and 1.0 μM native MAP2 (M2) (Sigma) in pellets (P) and supernatants (S) when incubated with 10 μM S-tubulin (ST). To ensure its stability during digestion, ~30 μM taxol was present with the S-tubulin. 1.0 μM MAP2 was also incubated with 10 μM control tubulin (Tu). (**C**) Pelleting assay to compare the binding to S-tubulin of 3R-tau purified by method 1 or method 2. (**D**) Binding of 3R-tau to normal tubulin in the absence or presence of kinesin motor domains (K). Results similar to those shown in (C) and (D) were obtained with 4R-tau.

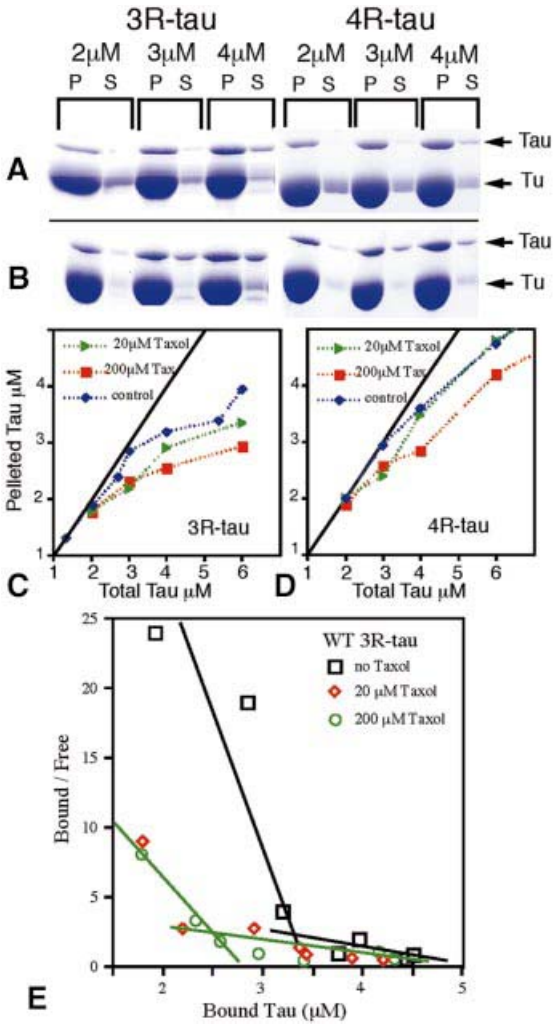

Fig. 4. Effect of taxol on tau binding. (**A** and **B**) SDS–polyacrylamide gels showing proteins in pellets (P) and supernatants (S) when 10 μM tubulin dimer was incubated with increasing concentrations of wild-type 3R-tau and 4R-tau in (A) the absence or (B) the presence of 20 μM taxol. Similar results were obtained for triple mutant 4R-tau, before and after labelling with nanogold (Figure 5). (**C** and **D**) Plots of pelleted WT tau measured by gel densitometry. A binding curve in the presence of 200 μM taxol is also included. (**E**) Scatchard plots of the results for 3R-tau showing the large change in the dissociation constant (inverse of the slopes of the lines) when excess tau is bound. In the absence of taxol, below 3 μM total tau there is so little in the supernatants that the slope of the strongly binding phase is not defined accurately by our data. There is even greater uncertainty for 4R-tau, which apparently binds more tightly (Supplementary data).

In further pelleting assays with normal tubulin, inclusion of 20 μM taxol increased the amount of tau in supernatants for both 3R-tau and 4R-tau (Figure 4A and B). For example, when 3 μM 3R-tau was mixed with 10 μM tubulin dimer, 20% less bound when taxol was present; for 3 μM 4R-tau, ~12% less bound in the presence of taxol. As a result, the binding curves make the break from the tight binding phase to the weaker binding phase at lower stoichiometries. The slope of the weak binding phase for 3R-tau is not changed significantly (Figure 4C). The behaviour of high concentrations of 4R-tau was more variable, for reasons that are unclear (Figure 4D). When the concentration of taxol was increased to 200 μM, the maximum that would dissolve, a little more tau appeared in some supernatants but concentrations of either type of tau up to 2 μM still bound quite strongly. Scatchard plots in the absence or presence of taxol approximate to two straight lines. The plot for 3R-tau (Figure 4E) shows that taxol reduces the affinity of the tight binding phase and also that the tau to tubulin dimer ratio at which the weaker binding phase takes over decreases to 1:5 (2 μM 3R-tau to 10 μM tubulin dimers) instead of 1:3. The Scatchard plot for 4R-tau (see Supplementary data available at *The EMBO Journal* Online) shows qualitatively similar changes.

To locate the binding site for the repeat motifs by electron microscopy, we made a triple mutant of 4R-tau with a single cysteine in R2 (see Figure 1B). The mutant tau was as efficient as wild-type 4R-tau in nucleating microtubules from soluble tubulin (data not shown) and the binding curve was also unchanged. Since we used the mutant 4R-tau for the nanogold experiments, we have shown the binding curves of this protein (Figure 2). Nucleation and binding were also unchanged when the cysteine of the mutant was labelled with nanogold (Figure 5C). We purified the labelled tau away from excess gold to avoid non-specific labelling (Figure 5A and B) and used it to polymerize microtubules for electron cryomicroscopy. Assembly was in the presence of TMAO and GMPCPP to help make well ordered specimens for computer analysis. We also tested that replacing GTP with GMPCPP made no difference to the way that tau bound to microtubules in the pelleting assay (Figure 5C).

Micrographs were taken of unstained frozen specimens (Figure 6A). Some gold particles can be seen easily (arrows) but others may be obscured by noise (Figure 6B). In any case, they are unlikely to appear in a regular pattern, since tau molecules cannot be arranged with proper helical

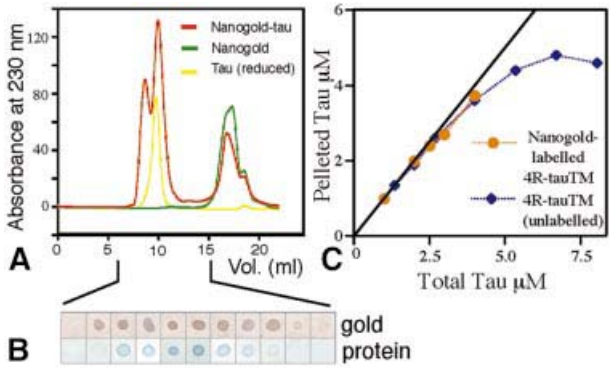

Fig. 5. (**A**) Separation of free nanogold from labelled protein by gel filtration (red curve). (**B**) Fractions of the first peak were dotted onto nitrocellulose paper and stained to detect the presence of gold and protein. The second peak (free gold without protein) did not bind to the paper. (**C**) Binding assays of labelled and unlabelled triple mutant tau (4R-tauTM). The curve shown is for assembly with GMPCPP; results for GTP were similar.

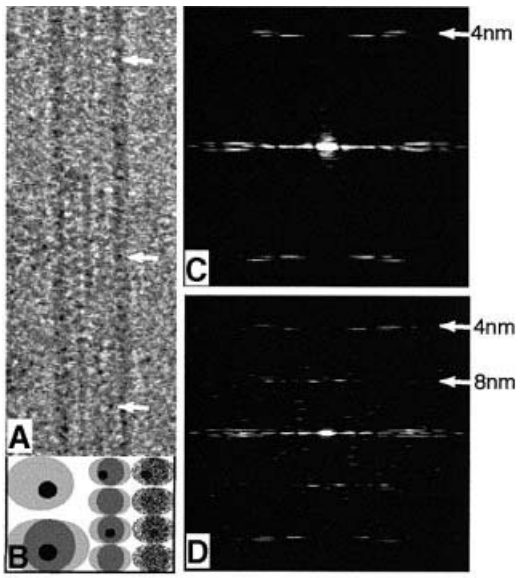

Fig. 6. (**A**) Electron micrograph of a frozen hydrated microtubule containing nanogold-labelled 4R-tauTM. Arrows indicate some of the gold particles that can be seen directly. (**B**) Model of a 15 kDa gold particle attached to a 50 kDa tubulin monomer (top left). In the image of a microtubule containing one labelled tau molecule per three to four tubulin dimers, a labelled monomer will usually be superimposed on an unlabelled monomer on the other side of the tube (lower left and centre). Noise in the image (right) makes some gold particles undetectable by eye. (**C** and **D**) Calculated diffraction patterns from electron microscope images of microtubules assembled with nanogold-labelled 4R-tauTM (C) without further decoration and (D) fully decorated with kinesin motor domains. The 4 nm layerline arises from the longitudinal spacing of tubulin monomers, and the 8 nm layerline from the binding of a kinesin molecule to each tubulin heterodimer (see Figure 7G).

symmetry in a 1:4 ratio on the tubulin dimer lattice. Images of 15-protofilament microtubules were processed by Fourier methods. Those that gave good diffraction patterns (e.g. Figure 6C) were used to produce reconstructed images. The reconstruction method depends on averaging different subunits to obtain different views and to reduce noise. Because the gold particles are not in a symmetrical arrangement, it is impossible to reconstruct a

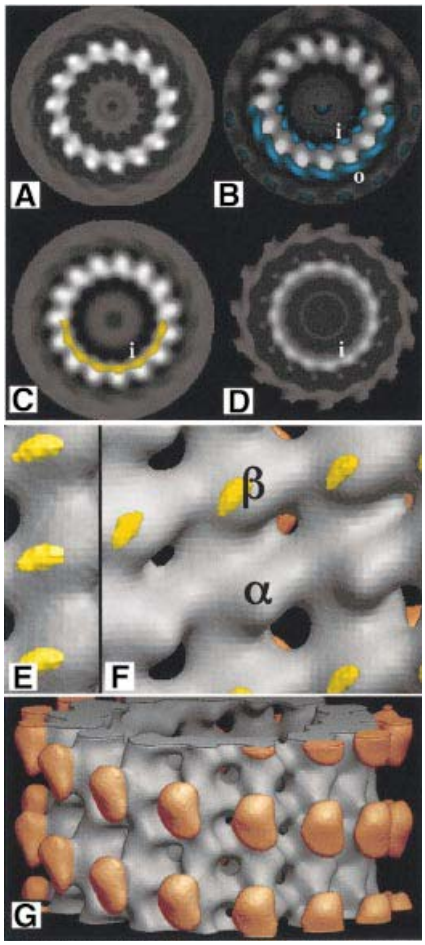

Fig. 7. Reconstructed images. (A–D) End-on views of microtubules without kinesin. (**A**) Pure tubulin (with GMPCPP). (**B**) Tubulin co-assembled with unlabelled tau. Tau difference density (at a lower cut-off level) is superimposed in blue on half of the map; some density appears on the inner (i) and outer (o) surfaces. (**C**) Tubulin co-assembled with labelled tau. The peak of the difference density due only to nanogold is superimposed in yellow. (**D**) Complete nanogold difference map [(C) minus (B)]. (E and F) Inside views of three-dimensional maps. (**E**) Three-dimensional version of (C). (**F**) As–sembled with labelled tau and decorated outside with kinesin (red). Peaks of the density difference between maps of kinesin-decorated microtubules containing labelled tau and without tau, are shown in yellow. (**G**) Outside view of kinesin-decorated microtubule assembled with gold-labelled tau. The difference map shows no density here at the level depicted in (F).

three-dimensional image in which one out of each eight tubulin monomers appears labelled. Instead, the label will appear at a reduced intensity on every subunit. We first reconstructed two-dimensional images (end-on views) to find the radial position of the gold label. The electron density maps of averaged end-on views of microtubules with unlabelled tau (Figure 7B) and nanogold-labelled tau (Figure 7C) appeared similar by eye, but difference maps (Figure 7D) reproducibly showed density corresponding to the gold label on the inside of the microtubule (Figure 7C, yellow). The peak density difference lies well outside the 99% confidence limit for random variance in individual maps. There were no significant differences on the outside. We then calculated three-dimensional maps in which every tubulin monomer was averaged and the difference

density appeared on each monomer close to where taxol binds to β-tubulin (Figure 7E).

Because the 8 nm layer-line data from the original images were too weak to appear above the noise, they could not be used to produce a distinction between α- and β-tubulin. Therefore we analysed images of gold-labelled microtubules decorated with kinesin, which produce a strong 8 nm layer-line (Figure 6D), making it possible to identify microtubules whose tubulin dimers are arranged with the perfect helical symmetry required for correct averaging. In these reconstructed three-dimensional images (Figure 7G) it is easy to identify β-tubulin from its position relative to kinesin (Amos and Hirose, 1997). The 15 kDa nanogold particles are actually present on one in four dimers, but every dimer is now averaged to reconstruct the image. Difference density (yellow) due to the gold label now peaks on β-tubulin (Figure 7F). Its position on the monomer is in good agreement with that already obtained independently for microtubules without kinesin (Figure 7E). In both cases, the label lies very close to the microtubule inner surface, suggesting that the 2 nm linker between the tau cysteine and the gold particle does not protrude normal to the surface and may even lie parallel to it.

Difference maps between microtubules without tau and with unlabelled tau in projection (Figure 7B, blue) show weak densities on both the inside and the outside of the microtubule. The difference density is noisy compared with the difference density for the gold label but is consistent with an extended molecule.

Discussion

Early work (reviewed by Chau *et al*., 1998) focused on the interaction of MAPs with the acidic C-terminal residues of tubulin, known to project flexibly from the outermost surface (Nogales *et al*., 1999). These residues inhibit microtubule assembly, presumably by charge repulsion, and if they are removed by subtilisin digestion, tubulin assembles more readily (Serrano *et al*., 1984). Similarly, positively charged molecules such as MAPs may promote assembly both by neutralizing the effect of the acidic tubulin C-termini and by linking other negatively charged regions of the outer surface. However, any positively charged molecule seems able to act in this way. A variety of proteins bind to microtubules, often linking them together into dense bundles (Melki *et al*., 1991), even if the C-terminal residues of tubulin are removed (Melki *et al*., 1991; Saoudi *et al*., 1995). Most previous studies of the binding of MAPs have involved microtubules that have been pre-assembled and stabilized with taxol; this must limit the ways in which tubulin and MAPs can interact. Our approach has been to co-assemble tubulin and tau together to allow tau molecules to become incorporated into their most natural positions in the microtubule structure.

The N-terminal domains of tau, MAP2 and MAP4 are known to project from the outer surfaces of microtubules. It is very likely that the adjacent region, the proline-rich segment, also binds only to the outer surfaces where it probably helps to stabilize the assembled state and produce the observed stiffening effect (Dye *et al*., 1993; Felgner *et al*., 1997). The binding of the proline-rich segment may be only partially specific since proline-rich domains are typically quite sticky and often bind non-stoichiometrically (Williamson, 1994). However, the fact that the repeat motifs are so well conserved suggests that their role is much more specific. Al-Bassam *et al*. (2002) have recently presented a model in which successive motifs of a tau or MAP2 molecule bind to adjacent tubulin monomers along the outer ridge of a single protofilament. However, these observations were made using tau added to preformed taxol-stabilized microtubules. Our data show that taxol affects the amounts of tau bound to microtubules. It is known that this drug stabilizes tubulin polymers by binding in a pocket between the 'M-loop' and the 'central helix' of β-tubulin (Amos and Löwe, 1999; Nogales *et al*., 1999). Taxol was not included in samples that we prepared for electron microscopy so that the binding site of the nanogold-labelled repeat motif would not be affected. The results have shown the gold label located on the inner surfaces of microtubules.

The image analysis process, as applied to microtubules, averages every tubulin subunit whether it is α or β, and whether it has gold bound to it or not. Enough of the subunits in the labelled microtubules had gold bound to them for it to appear at a lower level in the average. Thus we have been able to detect the label that was attached to the second repeat motif of 4R-tau, by subtracting the image of an unlabelled microtubule. The results clearly indicate that the labelled repeat motif is bound to the inside surface of a tubulin subunit. By repeating the image reconstruction with kinesin-decorated microtubules we have shown that the gold is attached to β- rather than α-tubulin. The simplest interpretation of both the effect of taxol in reducing the affinity between tau and tubulin and the positions of the gold labels in the three-dimensional images is that tau repeats bind to a site that overlaps with the taxol pocket. A possible alternative explanation for the effect of taxol is that its binding induces a conformational change in tubulin which affects tau binding to some other site inside or outside the microtubule. However, the location of the gold label makes this less likely. The sequence similarity between the repeat motifs and the loop stabilizing the conformation of α-tubulin also supports our interpretation.

The arrangement discovered by Al-Bassam *et al*. (2002) presumably occurs when a microtubule has already been assembled and stabilized either by taxol, as in their experiments, or by a sufficient number of other MAP molecules, as may occur *in vivo*. In fact, overexpression of tau in neurons has been shown to inhibit vesicle traffic along microtubules (Stamer *et al*., 2002), indicating that excess tau binds to the outsides of microtubules *in vivo*. However, the fact that 4R-tau has its extra motif inserted between the first and second motifs of 3R-tau (Figure 1) makes it unlikely that slight differences in the motifs specifically target them to α- or β-tubulin as suggested by Al-Bassam *et al*. (2002). We suggest that the differences between individual motifs produce grades of binding affinity to control the order in which they associate with a growing microtubule.

The saturating tau-to-tubulin ratio of 1:3 for the strongest binding phase of 3R-tau indicates that each repeat domain binds to one tubulin dimer. One might expect 4R-tau to saturate at a ratio of 1:4 but, counter to

this expectation, it saturates at a ratio of ~1:2.5. As well as its additional repeat motif, 4R-tau has the R1–R2 inter-repeat motif (Figure 1), which can bind strongly to taxol-stabilized microtubules as a lone peptide (Chau *et al*., 1998). Thus very strong binding is still possible when the average 4R-tau molecule has only ~2 repeat motifs bound to tubulin, probably R1 and R2, as well as the inter-repeat. Low concentrations of both 3R-tau and 4R-tau still bind strongly in the presence of taxol. The slopes of the initial lines in the Scatchard plots in the presence of taxol suggest a further binding mode that is quite strong, although weaker than the primary strong binding mode. In the case of 3R-tau (Figure 4E), for example, the Scatchard plot can be interpreted in terms of a region of tau, including at least one of the flanking regions, which attaches to five tubulin dimers. It is not yet clear whether this semi-strong mode of binding involves the inner or outer surfaces of the microtubules. The weak binding mode at higher concentrations probably consists of a mixture of non-optimal configurations, some of which might include binding to one or two sites on the inside as well as molecules attached only to the outside surface. At very high concentrations, tau molecules can also aggregate on top of each other on the microtubule surface (Ackmann *et al*., 2000).

Thus, our binding curves suggest that the very strongest binding is controlled by the repeat motifs and that the flanking regions play a secondary role. The repeats may bind well only in a particular conformation that can be disturbed by non-physiological conditions during purification and assembly. The presence of TMAO (Tseng and Graves, 1998) appears to make tau fold up into a better conformation against tubulin. One possible arrangement of the repeat domain is for successive repeats to lie along the shallow helices of tubulin monomers, linking three or four protofilaments together (Figure 8). The binding sites for PGGG loops within the repeat motifs (Figure 1) would then be on adjacent protofilaments, ~4 nm apart at this radius. This arrangement might explain why, under some conditions, a mixture of tubulin and MAPs assembles as rapidly growing protofilament triplets (Mandelkow *et al*., 1984). Alternatively, the repeat region may run along one protofilament, but in this case binding sites for the PGGG loops on β-tubulin would be ~8 nm apart and the inter-repeats would need to be fully stretched out between them.

Whilst observing dynamic instability, Ichihara *et al*. (2001) found that a local MAP2-to-tubulin dimer ratio of 1:16 stabilized segments of microtubule against depolymerization. It is likely that a similar ratio of MAPs, including tau, occurs *in vivo*. Thus only a minority of tubulin dimers will be occupied by repeat motifs and other regions of the microtubule-binding domain may have an important role as supplementary stabilizers. Part of the proline-rich flanking region (Figure 1) must provide the link between the N-terminal projection domain of tau on the outside of the microtubule and the repeat motifs on the inside surface; it could thread through one of the holes between the protofilaments. The N-terminal part of the microtubule-binding domain, attached to the projection, most probably runs along a protofilament. However, to trace the path of the complete molecule when incorporated into a microtubule in the absence of taxol will require labelling of several different residues. Our prediction is that, when a tau molecule is playing its full role, the repeat region runs across protofilaments to help stabilize lateral bonds and the flanking regions run along them to provide stiffening. But, apart from linking different protofilaments, we predict that the repeat motifs also directly stabilize the conformation of the β-tubulin monomers to which they bind, just as that of α-tubulin is stabilized by its own extra loop. A direct effect on the conformation of β-tubulin that could stabilize other dimers along the same protofilament by a cooperative mechanism, as suggested for taxol (Amos, 2000), could explain the substoichiometric effect of MAPs on microtubule stability.

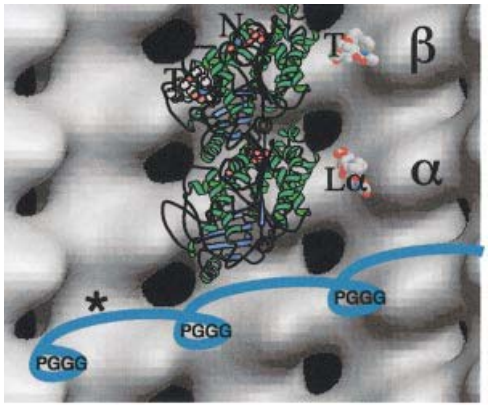

Fig. 8. Background: pure tubulin map (three-dimensional version of Figure 7A). Superimposed: ribbon diagram of αβ-tubulin atomic structure (PDB 1JFF) (Löwe *et al*., 2001). Lα, α-tubulin loop (T361–L368) alone; T, taxol; N, bound nucleotide. Blue structure, model of bound tau repeats including PGGG loops; the asterisk indicates an inter-repeat region.

Materials and methods

Mutants

Human 4R-tau was cloned into M13mp18 vector and mutations were introduced to replace Cys291, and Cys322 with isoleucine. Ser305 was replaced with cysteine. The mutated sequence was cloned into pRK172 and transformed into *Escherichia coli* BL21(DE3) cells for expression.

Spectroscopic analysis

6S tubulin, obtained as a lyophilized powder from Cytoskeleton, was resuspended in BRB80 (80 mM PIPES pH 6.9, 2 mM $MgCl_2$, 1 mM EGTA) and immediately refrozen in small aliquots on dry ice. 4R-tau protein was made up to 0.1 mg/ml in BRB80 with GTP and DTT (each 1 mM) and quickly mixed with freshly thawed tubulin to a final concentration of 1.0 mg/ml. The absorbance was determined at 350 nm and 37°C. 3R-tau was treated identically, but its final concentration was 0.3 mg/ml.

Tau purification method 1

Tau protein was expressed in *E.coli* strain BL21(DE3), and the bacterial pellet was lysed, spun at 15 300 *g* and the supernatant loaded onto a phosphocellulose column (Smith *et al*., 2000). The column was washed with 0.1 M NaCl in 50 mM PIPES, and the protein was eluted out with 0.3 M NaCl in 50 mM PIPES, passed through a 0.20 μm filter and dialysed overnight against saturated ammonium sulfate. The protein was precipitated twice in ammonium sulfate, resuspended in BRB80 and spun at 235 000 *g*. It was then boiled with 0.5 M NaCl–2% β-mercaptoethanol in BRB80 for 5 min, followed by chilling on ice, and gel filtrated through a Sephacryl S200 column prewashed with BRB80.

Tau purification method 2

Since tau normally co-purifies with lower molecular weight bands (probably degradation products), a faster method to yield purer tau was tried. Extracted protein was boiled immediately after grinding the bacterial pellet under liquid nitrogen. After a spin at 235 000 *g* the protein

was purified on a HiTrap SP column. The eluate was desalted on a Sephacryl S200 column. This protein appeared to be extremely pure, ran on SDS–PAGE in the same place as tau prepared by method 1 and was able to saturate microtubules in a similar manner, but it had only half the ability to nucleate tubulin polymerization (Figure 1). Possibly, as a result of the early boiling step, it had some RNA, DNA or another non-protein inhibitor (Bryan *et al*., 1975) bound to it.

Digestion of tubulin with subtilisin

S-tubulin was prepared as described (Chau *et al*., 1998), and the extent of digestion was assayed by western blotting with antibodies to the α- and β-tubulin C-termini, as well as to internal epitopes, and shown to be complete for both tubulin subunits (Figure 3A).

Pelleting assays

Tubulin was thawed from liquid nitrogen and spun at 77 300 *g* for 20 min. The protein concentration of the supernatants was determined spectroscopically. Since tau has a very low absorbance, its concentration was estimated by SDS–PAGE against a BSA standard and tau protein of known concentration. Different concentrations of tau (from 1.35 to 12 μM) were incubated with 10 or 20 μM tubulin, 0.1 M TMAO, 1 mM GTP and 5% dimethyl sulfoxide (DMSO), and incubated for 20 min at 37°C. After centrifugation at 96 600 *g* for 40 min, the supernatants were carefully removed and the pellets were resuspended in 40 μl of BRB80. Pellets and supernatants were run on SDS–PAGE, and the gels were stained with Page Blue 83. The concentration in each protein band was estimated using ImageQuant software. The assay was repeated at least three times for each type of tau and gave highly reproducible results, especially at fairly low ratios of tau to tubulin. In the absence of tubulin, no tau appeared in the pellet. For pelleting in the presence of paclitaxel (taxol), the drug was added prior to polymerization. We were able to dissolve up to 200 μM taxol since our buffer includes DMSO.

Nanogold labelling and electron cryomicroscopy

Maleimido-gold reagent (1.4 nm) was obtained from Nanoprobes, and 4R-tauTM was labelled at Cys305 following the supplier's protocol. Labelled tau was separated from an excess of free gold (Figure 5) on a Superdex-200 column run on an Äkta protein purifier (Amersham Pharmacia Biotech). Labelling was detected by silver-stained and protein-assayed dot blots of each fraction and spectroscopically at 280 and 420 nm. The latter measurements indicated that 93–97% of molecules were labelled. After separation from free gold, the labelled protein was incorporated immediately into microtubules. Tau from the 97%-labelled fraction was incubated with tubulin to final concentrations of 1.0 mg/ml tubulin, 0.3 mg/ml tau, 1 mM GMPCPP, 0.1 M TMAO and 5% DMSO at 37°C for 20 min. All grids were prepared within 3 days of labelling, after which the gold label has been shown to be unstable for some proteins. For some samples, 10 μM kinesin (rat KΔ340; Hirose *et al*., 1996) was added with 1 mM AMPPNP. Cryogrids were made and examined on a Philips CM-12, 120 KeV cryomicroscope at 45 000× magnification and 1.25 μm underfocus.

Image analysis

Micrographs were scanned in 28 μm steps and reconstructed using the MRC-LMB software package (Crowther *et al*., 1996; Hirose *et al*., 1996). Images of 15-protofilament microtubules were selected as their Fourier transforms contain distinct non-overlapping layer-lines (Figure 6C). In addition to reflections arising from the inter-protofilament spacing, the calculated Fourier transforms contained three layer-lines arising from the ~4 nm longitudinal spacing of tubulin monomers. Patterns from undecorated microtubules, with or without tau, contained traces of an 8 nm periodicity (Figure 6C) arising from the distinction between α- and β-tubulin subunits, but the data were too weak and noisy to be useful. Microtubules decorated with kinesin produced a group of three strong ~8 nm layer-lines (Figure 6D). Layer-line data from different images, to a resolution of ~3.5 nm, were compared and those that were in best agreement (Supplementary data) were averaged (at least 6000 nm of 15-pf microtubule, 12 000 tubulin dimers, 3000 tau molecules). Maps of different specimens were normalized (Trachtenberg and DeRosier, 1987) and difference maps calculated.

Supplementary data

Supplementary data are available at *The EMBO Journal* Online.

Acknowledgements

We thank John Berriman for much help with electron cryomicroscopy, Suzanne Cordell and Jan Löwe for help with chromatography, especially in the purification of gold-labelled tau and Maria Alonso for help with recombinant kinesin. S.K. is the recipient of a Cambridge Nehru Scholarship. L.A.A. thanks the Human Frontier Science Program for some financial support.

References

Ackmann,M., Wiech,H. and Mandelkow,E. (2000) Nonsaturable binding indicates clustering of tau on the microtubule surface in a paired helical filament-like conformation. *J. Biol. Chem.*, **275**, 30335–30343.

Al-Bassam,J., Ozer,R.S., Safer,D., Halpain,S. and Milligan,R.A. (2002) MAP2 and tau bind longitudinally along the outer ridges of microtubule protofilaments. *J. Cell Biol.*, **157**, 1187–1196.

Amos,L.A. (2000) Focusing-in on microtubules. *Curr. Opin. Struct. Biol.*, **10**, 236–241.

Amos,L.A. and Hirose,K. (1997) The structure of microtubule–motor complexes. *Curr. Opin. Cell Biol.*, **9**, 4–11.

Amos,L.A. and Löwe,J. (1999) How taxol stabilises microtubule structure. *Chem. Biol.*, **6**, R65–R69.

Bryan,J.,W., Nagle,B.W. and Doenges,K.H. (1975) Inhibition of tubulin assembly by RNA and other polyanions: evidence for a required protein. *Proc. Natl Acad. Sci. USA*, **72**, 3570–3574.

Chau,M.F., Radeke,M.J., deInés,C., Barasoain,I., Kohlstaedt,L.A. and Feinstein,S.C. (1998) The microtubule-associated protein tau cross-links to two distinct sites on each α and β tubulin monomer via separate domains. *Biochemistry*, **37**, 17692–17703.

Crowther,R.A., Henderson,R. and Smith,J.M. (1996) MRC image processing programs. *J. Struct. Biol.*, **116**, 9–16.

Dye,R.B., Fink,S.P. and Williams,R.C.J. (1993) Taxol-induced flexibility of microtubules and its reversal by MAP2 and Tau. *J. Biol. Chem.*, **268**, 6847–6850.

Felgner,H., Frank,R., Biernat,J., Mandelkow,E.-M., Mandelkow,E., Ludin,B., Matus,A. and Schliwa,M. (1997) Domains of neuronal microtubule-associated proteins and flexural rigidity of microtubules. *J. Cell Biol.*, **138**, 1067–1075.

Goedert,M., Baur,C.P., Ahringer,J., Jakes,R., Hasegawa,M., Spillantini,M.G., Smith,M.J. and Hill,F. (1996) PTL-1, a microtubule-associated protein with tau-like repeats from the nematode *Caenorhabditis elegans*. *J. Cell Sci.*, **109**, 2661–2672.

Gustke,N., Trinczek,B., Biernat,J., Mandelkow,E.M. and Mandelkow,E. (1994) Domains of tau-protein and interactions with microtubules. *Biochemistry*, **33**, 9511–9522.

Hasegawa,M., Smith,M.J. and Goedert,M. (1998) Tau proteins with FTDP-17 mutations have a reduced ability to promote microtubule assembly. *FEBS Lett.*, **437**, 207–210.

Heidary,G. and Fortini,M.E. (2001) Identification and characterization of the *Drosophila* tau homolog. *Mech. Dev.*, **108**, 171–178.

Hirokawa,N., Shiomura,Y. and Okabe,S. (1988) Tau proteins—the molecular-structure and mode of binding on microtubules. *J. Cell Biol.*, **107**, 1449–1459.

Hirose,K., Lockhart,A., Cross,R.A. and Amos,L.A. (1996) Three-dimensional cryoelectron microscopy of dimeric kinesin and ncd motor domains on microtubules. *Proc. Natl Acad. Sci. USA*, **93**, 9539–9544.

Hutton,M. *et al*. (1998) Association of missense and 5′-splice-site mutations in *tau* with the inherited dementia FTDP-17. *Nature*, **393**, 702–705.

Hyman,A.A., Salser,S., Drechsel,D.N., Unwin,N. and Mitchison,T.J. (1992) Role of GTP hydrolysis in microtubule dynamics: information from a slowly hydrolyzable analogue, GMPCPP. *Mol. Biol. Cell*, **3**, 1155–1167.

Ichihara,K., Kitazawa,H., Iguchi,Y., Hotani,H. and Itoh,T.J. (2001) Visualization of the stop of microtubule depolymerization that occurs at the high-density region of microtubule-associated protein 2 (MAP2). *J. Mol. Biol.*, **312**, 107–118.

Lee,V.M.-Y., Goedert,M. and Trojanowski,J.Q. (2001) Neurodegenerative tauopathies. *Annu. Rev. Neurosci.*, **24**, 1121–1159.

Littauer,U.Z., Giveon,D., Thierauf,M., Ginzburg,I. and Ponstingl,H. (1986) Common and distinct tubulin binding sites for microtubule-associated proteins. *Proc. Natl Acad. Sci. USA*, **83**, 7162–7166.

Löwe,J., Li,H., Downing,K.H. and Nogales,E. (2001) Refined structure of αβ tubulin at 3.5 Å resolution. *J. Mol. Biol.*, **313**, 1045–1057.
Mandelkow,E., Schultheiss,R. and Mandelkow,E.M. (1984) Assembly and 3-dimensional image-reconstruction of tubulin hoops. *J. Mol. Biol.*, **177**, 507–529.
Melki,R., Kerjan,P., Waller,J.-P., Carlier,M.-F. and Pantaloni,D. (1991) Interaction of microtubule-associated proteins with microtubules: yeast lysyl- and valyl-tRNA synthetases and tau 218–235 synthetic peptide as model systems. *Biochemistry*, **30**, 11536–11545.
Nogales,E., Whittaker,M., Milligan,R.A. and Downing,K.H. (1999) High resolution model of the microtubule. *Cell*, **96**, 79–88.
Poorkaj,P. *et al*. (1998) Tau is a candidate gene for chromosome 17 frontotemporal dementia. *Ann. Neurol.*, **43**, 815–825.
Saoudi,Y., Paintrand,I., Multigner,L. and Job,D. (1995) Stabilization and bundling of subtilisin-treated microtubules induced by microtubule associated proteins. *J. Cell Sci.*, **108**, 357–367.
Serrano,L., Avila,J. and Maccioni,R.B. (1984) Controlled proteolysis of tubulin by subtilisin—localization of the site for MAP2 interaction. *Biochemistry*, **23**, 4675–4681.
Smith,M.J., Crowther,R.A. and Goedert,M. (2000) The natural osmolyte trimethylamine *N*-oxide (TMAO) restores the ability of mutant tau to promote microtubule assembly. *FEBS Lett.*, **484**, 265–270.
Spillantini,M.G. *et al*. (1998) Mutation in the tau gene in familial multiple system tauopathy with presenile dementia. *Proc. Natl Acad. Sci. USA*, **95**, 7737–7741.
Stamer,K., Vogel,R., Thies,E., Mandelkow,E. and Mandelkow,E.-M. (2002) Tau blocks traffic of organelles, neurofilaments and APP vesicles in neurons and enhances oxidative stress. *J. Cell Biol.*, **156**, 1051–1063.
Takei,Y., Teng,J., Harada,A. and Hirokawa,N. (2000) Defects in axonal elongation and neuronal migration in mice with disrupted *tau* and *map*1b genes. *J Cell Biol.*, **150**, 989–1000.
Trachtenberg,S. and DeRosier,D.J. (1987) Three-dimensional structure of the frozen-hydrated flagellar filament. The left-handed filament of *Salmonella typhimurium. J. Mol. Biol.*, **195**, 581–601.
Trinczek,B., Biernat,J., Baumann,K., Mandelkow,E.M. and Mandelkow,E. (1995) Domains of tau-protein, differential phosphorylation and dynamic instability of microtubules. *Mol. Biol. Cell*, **6**, 1887–1902.
Tseng,H.-C. and Graves,D.J. (1998) Natural methylamine osmolytes, trimethylamine *N*-oxide and betaine, increase tau-induced polymerization of microtubules. *Biochem. Biophys. Res. Commun.*, **250**, 726–730.
Williamson,M.P. (1994) The structure and function of proline-rich regions in proteins. *Biochem. J.*, **297**, 249–260.

Received July 15, 2002; revised September 25, 2002; accepted October 31, 2002